Process Monitoring and Fault Detection on a Hot Melt Extrusion Process using In-line Raman Spectroscopy and a Hybrid Soft Sensor

Furqan Tahir, Muhammad T. Islam, John Mack, John Robertson, David Lovett

PII: S0098-1354(18)30460-5
DOI: https://doi.org/10.1016/j.compchemeng.2019.03.019
Reference: CACE 6380

To appear in: *Computers and Chemical Engineering*

Received date: 14 May 2018
Revised date: 28 January 2019
Accepted date: 13 March 2019

Please cite this article as: Furqan Tahir, Muhammad T. Islam, John Mack, John Robertson, David Lovett, Process Monitoring and Fault Detection on a Hot Melt Extrusion Process using In-line Raman Spectroscopy and a Hybrid Soft Sensor, *Computers and Chemical Engineering* (2019), doi: https://doi.org/10.1016/j.compchemeng.2019.03.019

Highlights

- Real-time process monitoring scheme proposed for pharmaceutical Hot Melt Extruder.
- A PLS calibration model (using inline Raman spectra) predicts API concentration.
- A Hybrid soft sensor (using feeder process data) also predicts API concentration.
- PCA and SPC monitors designed using the above two independent sensor predictions.
- This two-sensor scheme detects various HME faults which a one-sensor scheme cannot.

Process Monitoring and Fault Detection on a Hot Melt Extrusion Process using In-line Raman Spectroscopy and a Hybrid Soft Sensor

Furqan Tahir[a,*], Muhammad T. Islam[b], John Mack[a], John Robertson[b], David Lovett[a]

[a] *Perceptive Engineering Ltd, Vanguard House, Sci Tech Daresbury, Cheshire WA4 4AB, UK*

[b] *EPSRC Centre for Innovative Manufacturing in Continuous Manufacturing and Crystallisation, University of Strathclyde, Glasgow G1 1RD, UK*

Abstract

We propose a real-time process monitoring and fault detection scheme for a pharmaceutical hot melt extrusion process producing Paracetamol-Affinisol extrudate. The scheme involves prediction of Paracetamol concentration from two independent sources: a hybrid soft sensor and a Raman-based Partial Least Squares (PLS) calibration model. Both these predictions are used by the developed PCA (Principal Component Analysis) and SPC (Statistical Process Control) monitors to detect process faults and raise alarms. Through real-time extrusion results, it is shown that this two-sensor approach enables the detection of various common process faults which would otherwise remain undetected with a single-sensor monitoring scheme.

Keywords: Process Monitoring, Fault Detection, Hot Melt Extrusion, PCA, PLS, Calibration Model, Hybrid Soft Sensor, Affinisol, HPMC

*Corresponding author.
Email addresses: ftahir@perceptiveapc.com, ftahir49@hotmail.com (Furqan Tahir), tariq.islam@strath.ac.uk (Muhammad T. Islam), jmack@perceptiveapc.com (John Mack), j.robertson@strath.ac.uk (John Robertson), dlovett@perceptiveapc.com (David Lovett)

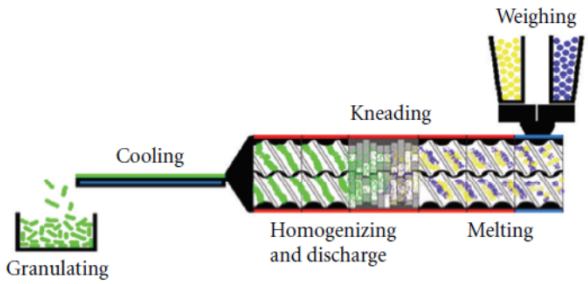

Figure 1: HME process overview [1]

1. Introduction

Hot Melt Extrusion (HME) is one of the most widely used processing techniques within the plastic and rubber manufacturing industry as well as the food processing industry. More recently, HME has attracted significant interest from the pharmaceutical sector [1]. This is because HME enables *continuous* manufacture of a wide variety of dosage forms including solid dose formulations, which are useful in the context of poorly soluble APIs (see e.g. [2] and the references therein). Furthermore, through the incorporation of suitable inline Process Analytical Technology (PAT) [3],[4], HME facilitates the 'Quality by Design' (QbD) approach to pharmaceutical manufacturing by enabling continuous process monitoring and control [2]. The HME drug delivery system is also versatile in that it can be used to produce granules, pellets, tablets, capsules, implants, stents, transdermal and ophthalmic inserts [5].

The pharmaceutical HME process involves feeding of API (Active Pharmaceutical Ingredient) and excipient powders into the HME barrel. The barrel typically houses two screws (rotated by a motor), and is divided into sections called zones. Each zone has its own heating and cooling unit with a thermocouple (for temperature control and measurement) and, depending on the corresponding screw type, can either be classed as a kneading (mixing) zone or conveying (transport) zone. As shown in Figure 1, the powder blend is melted in the first few zones, followed by kneading to mix the melt, homogenisation

and then discharge (through the die zone) for further processing downstream [6], [1].

For monitoring and fault detection of various processes, a common tool is the so-called soft sensor - see [7] for a comprehensive review of soft sensors within the process industry. These soft sensors, which can be model-driven or data-driven, are used to predict the critical quality attributes [8]. Furthermore, in conjunction with other techniques such as Principal Component Analysis (PCA), they can be used to monitor processes as well as identifying various faults (see e.g. [9] [10] and the references therein).

In the context of HME processing, Raman spectroscopy - consisting of a fibre optic probe connected to a spectrometer - has been used to monitor drug formulation to achieve QbD manufacturing requirements (see e.g. [11] and the references therein). In [12], Raman spectroscopy was used for on-line analysis to quantify the drug loading (API concentration) in hot-melt extruded films and to evaluate the physical state of chemicals within the formulation. Furthermore, PLS (Partial Least Squares) models were developed by regressing the on-line Raman spectra against the API concentration. Similarly, in [13], an in-line Raman was employed within the die zone of a 16 mm co-rotating twin-screw extruder to monitor and predict the drug content and to evaluate the solid state of the extrudates prior to discharge. A PLS model was also designed and validated to predict the API concentration. In-line Raman spectroscopy was also used in [14] to monitor and evaluate the materials behaviour at a molecular level during the extrusion as a function of process parameters, i.e. temperature and screw speed. Through PCA, it was observed that increasing barrel temperature reduced the crystallinity of the API within the extrudate. Results on in-line barrel monitoring to improve the material understanding and impact of processing conditions within the HME were also reported in [15].

As discussed above, most of the work in the literature involving Raman spectroscopy has focused on monitoring/understanding the chemical composition and drug interactions of the extrudate within HME. In this paper, however, we address the problem of HME monitoring and fault detection from a process

viewpoint. In particular, a scheme to detect typical operational faults during HME processing (e.g. zone heater failures, powder feeding issues and Raman probe exposure faults) is proposed. Through real-time results, we show that a PLS calibration model (predicting API concentration using in-line Raman spectra) on its own is not sufficient to detect the aforementioned faults. To remedy this, we also design a back-up (hybrid) soft sensor [16, 7]. API concentration predictions from these two independent sources, as well as the process data, are then fed into the developed PCA and SPC (Statistical Process Control) monitors. As demonstrated by real-time results (section 4), such an arrangement of two independent soft sensors, together with the PCA/SPC monitors, enables the proposed scheme to pick up a wide range of HME process faults (which a single-sensor based monitoring scheme cannot).

This paper is organised as follows: Section 2 provides a description of the experimental setup and method. The proposed process monitoring scheme (including the design of calibration model, soft sensor, PCA and SPC monitors) is formulated in Section 3. Real-time HME process monitoring results are presented in Section 4 and the conclusion is given in Section 5. A proof sketch of the soft sensor model transfer function is provided in the Appendix.

1.1. Abbreviations

- **API**: Active Pharmaceutical Ingredient
- **CSTR**: Continuous Stirred-Tank Reactor
- **DoE**: Design of Experiment
- **FOPTD**: First Order Plus Time Delay
- **HME**: Hot Melt Extrusion
- **NIR**: Near-Infrared
- **OPC**: OLE for Process Control
- **PAT**: Process Analytical Technology
- **PCA**: Principal Component Analysis
- **PLC**: Programmable Logic Controller
- **PLS**: Partial Least Squares
- **PV**: Process Value

- **QbD**: Quality by Design
- **RMSEE**: Root Mean Squared Error of Estimation
- **SP**: Setpoint Value
- **SNV**: Standard Normal Variate
- **SPC**: Statistical Process Control
- **SPE**: Squared Prediction Error
- **LCL**: Lower Control Limit
- **LWL**: Lower Warning Limit
- **LV**: Latent Variable
- **UCL**: Upper Control Limit
- **UWL**: Upper Warning Limit

2. Experimental Setup and Method

This section provides a description of the experimental setup including the HME unit, powder feeders and Raman spectrometer as well as the software package used for implementing the proposed monitoring scheme.

2.1. Hot Melt Extruder and Feeder Units

Hot melt extrusion was carried out using EuroLab 16, a 16mm barrel-diameter co-rotating twin-screw extruder from Thermo-Fisher Scientific [17].

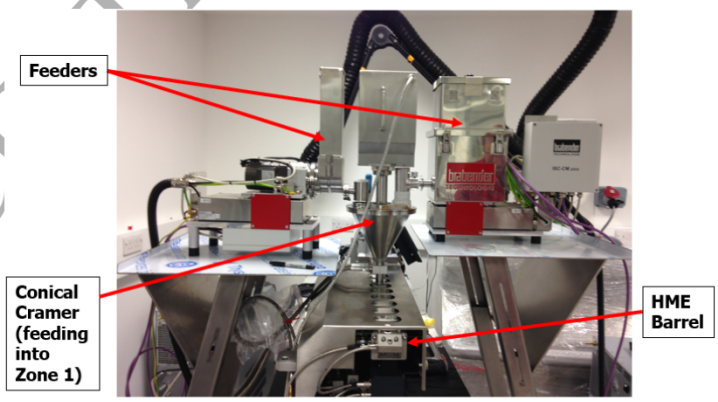

Figure 2: HME and feeder setup

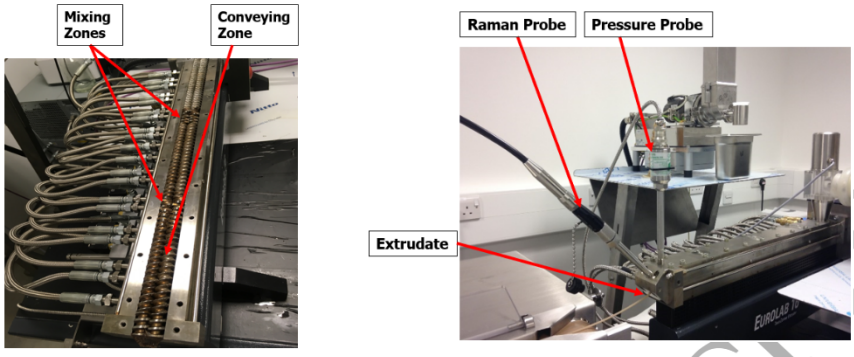

(a) Screws in the HME barrel

(b) In-line Raman probe

Figure 3: HME screws and in-line Raman probe setup

The ratio of the screw length to barrel diameter (L/D ratio) is 40:1 and the extruder barrel consists of 10 heating zones plus a die zone. The experimental setup is shown in Figure 2.

API (Paracetamol powder) and excipient (Affinisol powder) were fed into the HME through two Loss-in-weight feeders, which have load cells to calculate the loss in weight of powder and hence support gravimetric feeding (closed loop) [18]. The feeders used in this study were FlexWall DDW-FW20 and MiniTwin DDW-MT from Brabender Technology [19]. These feeders discharge into zone 1 of the barrel. The co-rotating screws mix the materials and transport the melt, through the barrel, towards the die zone for extrusion. The HME screw configuration used in this study is shown in Figure 3a. It consisted of two mixing zones (with 30°, 60° and 90° kneading elements) and 8 conveying (transport) zones. The EuroLab 16 unit can heat up to 300°C (in each zone) and the HME motor supports a maximum screw speed of 1000 rpm.

2.2. In-line Raman Spectroscopy

In-line Raman spectra were collected using the Raman Rxn2 spectrometer from Kaiser Optical Systems Inc [20]. For in-line measurements, a fibre-optic Raman Dynisco probe was connected into the die head (Figure 3b), to monitor the API concentration of the melt before it is extruded out through the die.

The employed laser wavelength of 785 nm was generated from an Invictus NIR (near-infrared) diode laser [20]. All in-line spectra were logged with a resolution of 4 cm^{-1}, an exposure time of 10 seconds and using a laser power of 350 mW. Raman spectra was collected at a sampling interval of 15 seconds. Furthermore, at the start of each experiment, a 10 minute process/spectra stabilization time was considered before commencing the API feed.

2.3. PharmaMV software

The proposed monitoring and fault detection scheme was developed and deployed, in real-time, using PharmaMV software package from Perceptive Engineering Limited [21]. Communication was implemented between PharmaMV and the HME PLC (programmable logic controller) unit using an OPC (OLE for Process Control) interface [22]. This interface enabled PharmaMV to log all the process variables (e.g. temperatures, motor torque and power, pressure) as well as write the setpoints (SP) such as screw speed, zone temperatures and feed rates. The in-line Raman spectral data was also collected and time-aligned with the process data in PharmaMV to run the SPC, PCA and PLS models in real-time.

2.4. PCA and PLS Algorithms

The models developed in this work involve the use of PCA and PLS algorithms which are summarised below.

PCA is a statistical, dimensional-reduction technique which has extensively been used for process monitoring (see e.g. [23], [24], [25], [26]) as well as control (see e.g. [27] [28]). PCA algorithm typically involves performing singular value decomposition on the (normalised) data covariance matrix, breaking it down into two orthogonal matrices, know as loading matrices, and a diagonal matrix that contains the eigenvalues. The loading matrix is used to project the original data onto the so-called latent variable (LV) space, resulting in a model of the form:

$$X = TP^T + E \tag{1}$$

where X, T, P and E are the data, score, loading and residual matrices respectively.

The first LV describes the direction of greatest variation within the dataset. As each LV successively describes less information, a number of lower LVs are ignored by the user as they represent noise and hence the dimensionality of the problem is reduced. Note that the variation described by each LV is proportional to the magnitude of its associated eigenvalue.

In the context of process monitoring, two important metrics associated with the PCA model are the SPE (squared prediction error) [29] and T^2 thresholds, which are computed alongside the model. An SPE value above its threshold indicates a breakdown in the data correlation (which is reflective of potential process faults). Similarly, a T^2 value [30], when compared to its threshold, is indicative of process operation away from the mean (potentially highlighting faulty behaviour). Further details on the PCA algorithm, including mathematical formulation, are given in [31], [23].

PLS regression is also a data driven technique that has been extensively used for process monitoring as well as control design (see e.g. [23], [28] and the references therein). Through PLS, in a manner similar to the PCA algorithm, the (normalised) data predictors (X) and responses (Y) can be represented in the form [32]:

$$X = TP^T + E \tag{2a}$$

$$Y = UQ^T + F \tag{2b}$$

where P and Q are the loading matrices, T and U are the score matrices, and E and F are the residual matrices, for X and Y, respectively. The score matrices are computed such that $T = XW$ and $U = T\beta$, where W matrix is the regressor of X onto the associated (reduced-dimensional) LV space and β is the regressor of the X score space onto the Y score space. It follows from equation (2) that a closed-form regression relationship between the predictors and responses can then be given by

$$Y = XB + F \tag{3}$$

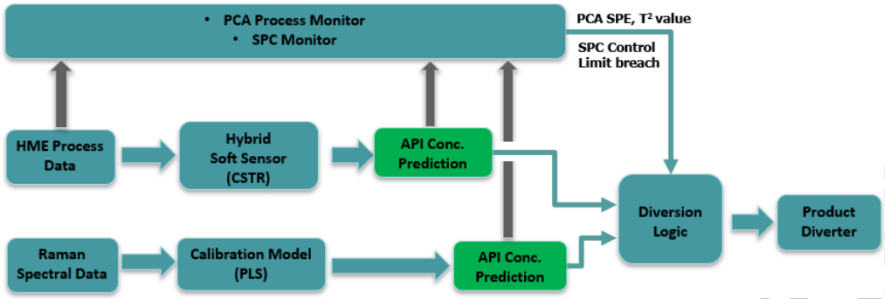

Figure 4: Proposed HME process monitoring scheme

where $B = W\beta Q^T$ is the matrix of coefficients identified by the PLS algorithm. For further details on the algorithm, see e.g. [31], [32], [33] and the references therein).

3. HME Process Monitor Development

In this section, we present the development of the HME process monitoring scheme. As shown in Figure 4, the proposed scheme involves real-time API concentration predictions from two independent source: a Raman calibration model as well as a CSTR (Continuous Stirred-Tank Reactor) soft sensor. These predictions (along with HME process data) are then used by the (developed) SPC and PCA models to monitor the process. Finally, the output from these models, namely SPE value and control limit violations, can then be used to divert any out-of-specification product and/or rectify process faults on the HME unit.

Design of Experiment (DoE) type tests were performed on the HME process to collect statistically rich data for developing the aforementioned models. As shown in Table 1, three sets of experiments were conducted at medium (200rpm), low (100rpm) and high (300rpm) screw speeds, respectively. In each set, the API and Excipient feedrates were varied to achieve a steady-state API concentration (based on the feedrate ratios) of 10 to 50% with increments of 10%. Notice that for set 3, due to the high screw speed, the total product throughput was

Set	Excipient Feedrate (Kg/hr)	API Feedrate (Kg/hr)	Steady-State Concentration (%)	Total Throughput (Kg/hr)	Screw Speed (RPM)	Temperature (Deg C)
1	0.9	0.1	10	1	200	180
1	0.8	0.2	20	1	200	180
1	0.7	0.3	30	1	200	180
1	0.6	0.4	40	1	200	180
1	0.5	0.5	50	1	200	180
2	0.9	0.1	10	1	100	160
2	0.8	0.2	20	1	100	160
2	0.7	0.3	30	1	100	160
2	0.6	0.4	40	1	100	160
2	0.5	0.5	50	1	100	160
3	1.35	0.15	10	1.5	300	160
3	1.2	0.3	20	1.5	300	160
3	1.05	0.45	30	1.5	300	160
3	0.9	0.6	40	1.5	300	160
3	0.75	0.75	50	1.5	300	160

Table 1: DoE runs on the HME process

increased to 1.5 kg/hr, primarily to prevent the HME from running partially empty.

To ensure good representation of the HME process, the training data for the PLS Calibration and CSTR soft sensor models was selected to include all five concentration levels. Similarly, for PCA and SPC monitors, data from all three DoE sets was included for robust model development.

3.1. Raman Calibration Model Design

During the DoE runs, Raman PAT spectra was collected in real-time, towards the HME exit in the die zone (see Figure 3b above). The spectra was pre-processed using Standard Normal Variate (SNV), to normalise the spectra around its mean, followed by Savitzky Golay filter (with window size 10, polynomial order of 2 and derivative order of 1) to remove additive effects and smooth out the spectra. A review of these pre-processing techniques can be found in [34].

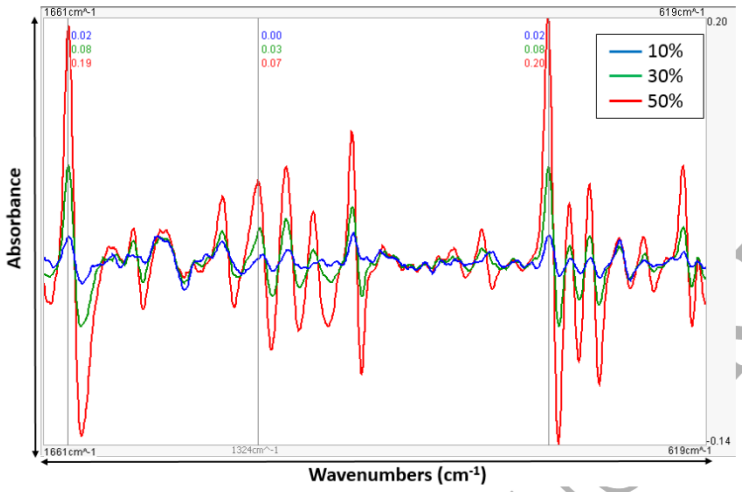

Figure 5: Raman spectra for Paracetamol at different concentrations

Figure 5 shows the pre-processed Raman spectra, between the wavenumbers 1661 cm^{-1} and 619 cm^{-1}, for API concentration of 10% (blue), 30% (green) and 50% (red), respectively. The spectra peaks are due to the presence of various chemical groups, such as the amide groups and C-C ring stretching (further details on the characteristic Paracetamol Raman spectra are given in [35], [36] and [37]). Figure 6 shows the strong correlation between Paracetamol concentration (10%-50%) and spectra amplitude around two such peak (867 cm^{-1} and 1622 cm^{-1}, respectively).

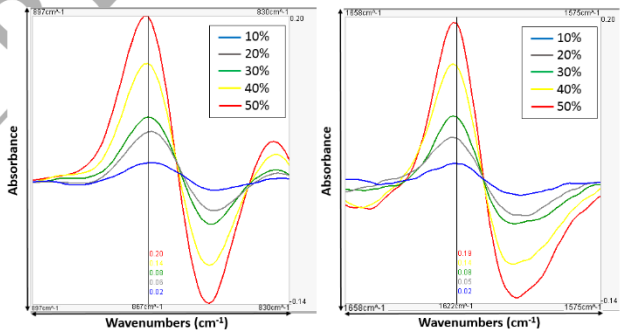

Figure 6: Raman peaks at 867 cm^{-1} (left) and 1622 cm^{-1} for different concentrations

Predictors (X)	Response (Y)	Latent Variable	R^2	Cumulative R^2
Pre-processed Raman Spectra	API % Concentration	1	73 %	73%
bins 1890 cm^{-1} to 150 cm^{-1}		2	14 %	87%
(1741 predictors in total)		3	4 %	91%

Table 2: PLS model variables and LV contributions

Using PharmaMV software package [21], a PLS calibration model was developed to predict, in real-time, the API % concentration, using the (pre-processed) Raman spectra corresponding to the wavenumber range: 1890cm^{-1} to 150cm^{-1} (1741 predictors in total). For the PLS model design, 3 LVs were selected which cumulatively accounted for 91% of the variability within the data (see Table 2). Figure 7 shows a good match between the calibration model predictions (blue trace on the first plot) and the theoretical API concentration based on the API-to-Total Feedrate ratios (given in red). The API and Excipient Feedrates plots are also shown on the figure for reference.

Remark 1. *Note that choosing more than 3 LVs overfitted the PLS model, thus capturing the noise and degrading the predictive performance on unseen data.*

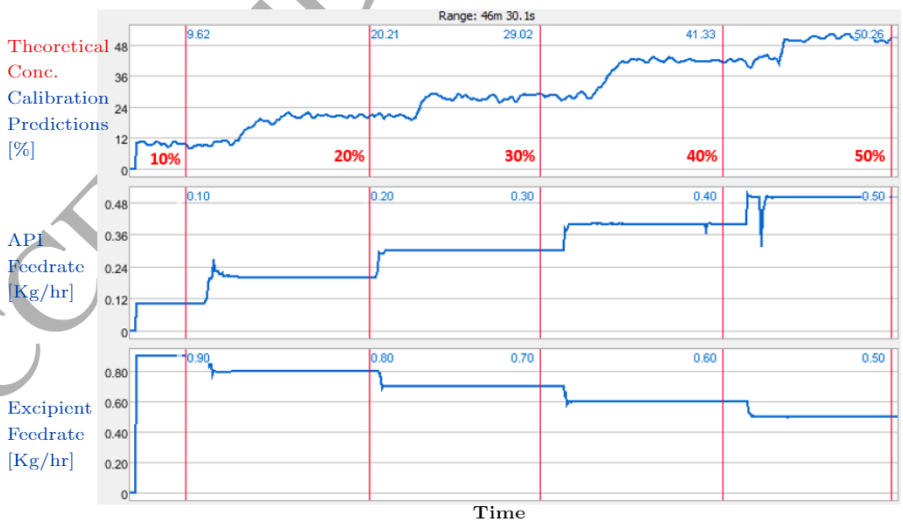

Figure 7: Raman calibration model design

3.2. Hybrid Soft Sensor Design

In this section, we present the development of a hybrid soft sensor to predict the dynamic API concentration at the outlet of the extruder using feeder process data.

By considering the component mass balance [38] as well as well as the propagation delay through the HME, the API outlet concentration can be modelling using a first-order plus time delay (FOPTD) transfer function:

$$G(s) = \frac{C^p_{out}(s)}{C_{in}(s)} = \frac{Ke^{-ds}}{Ts+1} \tag{4}$$

where C_{in} denotes the HME inlet API concentration ratio (unitless) and C^p_{out} is the percentage outlet API concentration (a proof sketch for $G(s)$ is provided in the Appendix). The model is hybrid in the sense that parameters K, d and T are identified, using the experimental calibration data for training (shown in Figure 7), through the Prediction Error Minimization method (PEM) [39]. PEM represents a family of identification algorithms which compute parameter estimates that minimize the prediction error. In this work, least squares identification was used on DoE Set 1 data to compute a model with the parameters:

$$K = 102.71, \quad T = 31.642, \quad d = 91.508 \tag{5}$$

yielding an R^2 value of 97%. The model was then discretised, at the sampling interval of $5s$, using Zero-Order Hold. The concentration predictions of this hybrid soft sensor, using real-time C_{in} data, are shown in Figure 8 (red trace on the first plot). Note that DoE sets 2 and 3 were used for validating the soft sensor. The figure shows a good match between the predictions of the calibration model and hybrid soft sensor across all three sets of data.

Remark 2. *Introducing K as a variable in model (4) provides the identification algorithm with an extra degree of freedom to reduce the prediction error. In the estimation algorithm, the initial guess of K was specified as* 100 *(as it is used to convert the API concentration ratio to a % - see the Appendix) but the final*

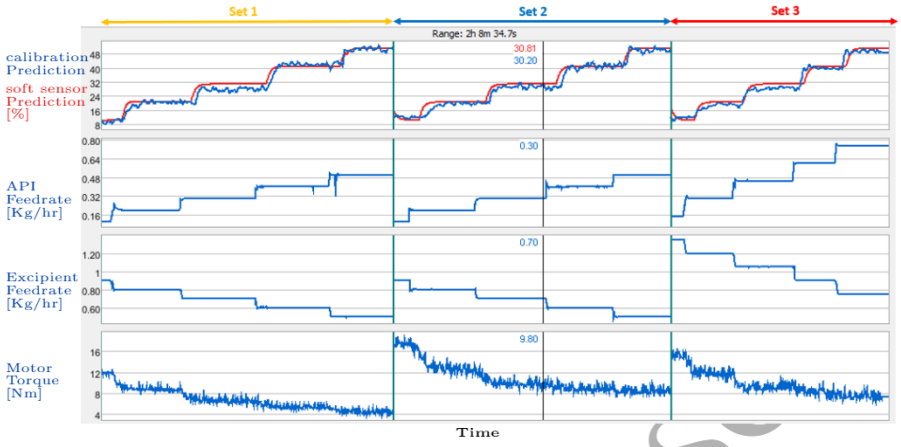

Figure 8: Training and validation data for hybrid soft sensor model development

Latent Variable	R^2	Cumulative R^2
1	75 %	75%
2	15 %	90%

Table 3: PCA LV contributions

value of 102.71 *was identified since calibration model predictions were used for training (which in themselves contain some prediction error).*

3.3. SPC and PCA Monitor Development

Having developed and validated the calibration model and soft sensor using the DoE data (Table 1), a PCA monitor as well as an SPC monitor were developed to detect HME process faults.

A 2-LV PCA monitor was developed in PharmaMV software package, capturing 90% of the variability within the data without overfitting or modelling the process noise, particularly in the torque signal (Table 3). The model used predictions from both PAT calibration model and the soft sensor, as well as excipient/API feedrates and motor torque data. Table 4 gives the model variables, the LV loadings and the predictions errors, whereas the PCA reconstructions of the training dataset are shown in Figure 9.

Variable	LV1 Loading	LV2 Loading	RMSEE (Normalised)
PAT Predictions	-0.512	0.094	0.211
CSTR Predictions	-0.457	0.251	0.448
Excipient Feedrate	0.384	0.745	0.261
API Feedrate	-0.438	0.549	0.299
Motor Torque	0.435	0.269	0.512

Table 4: PCA model variables, LV loadings and prediction errors

It can be seen in Table 4 that the second LV primarily describes the variation in the two feedrates (and therefore the total feedrate). This is clearly reflected in the score plot in Figure 10a, where the Set 3 data forms a separate cluster as the higher throughput results in larger score values for LV2 (Y-axis).

Finally, Figure 10b shows the computed SPE and T^2 thresholds (Alarm Limits) as well as values for the training dataset.

In addition to PCA and PLS, another important process monitoring tool is so-called statistical process control (SPC) [40]. SPC charts are typically used to monitor key process variables, online, to ensure that they remain within a

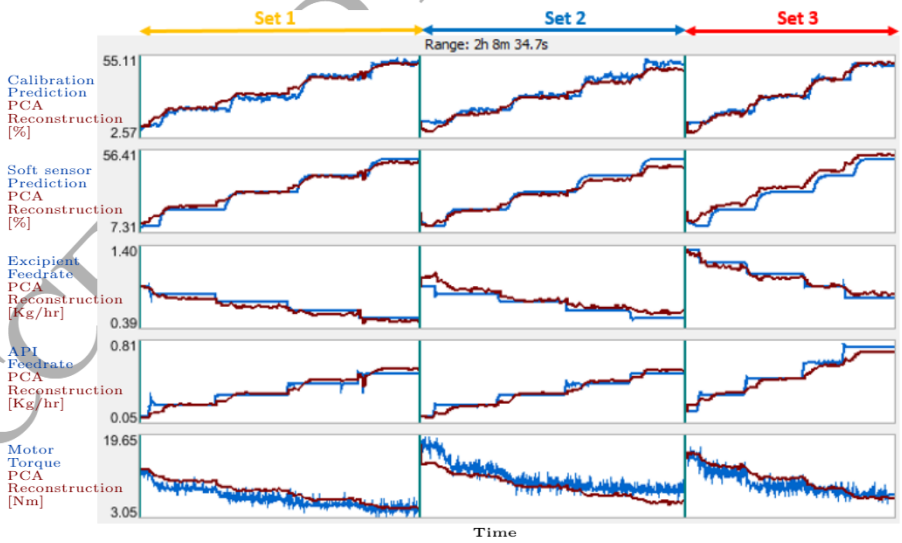

Figure 9: PCA monitor development - signal reconstructions

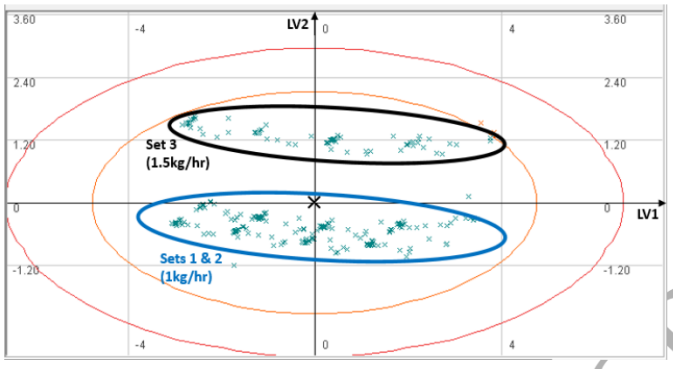

(a) PCA model score plot

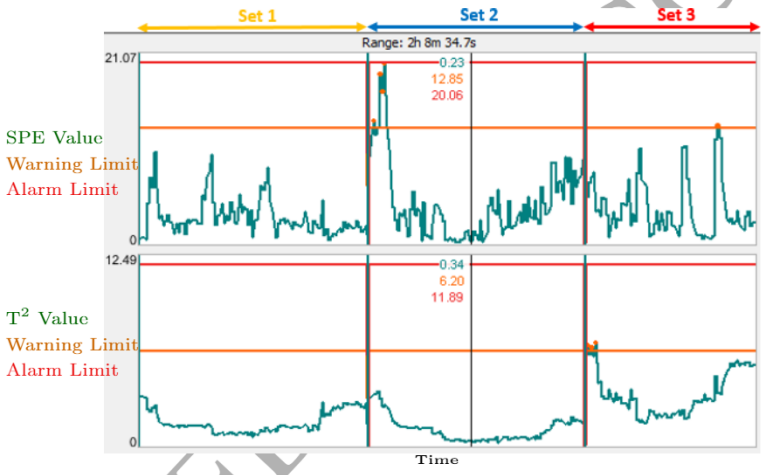

(b) PCA model SPE and T^2

Figure 10: PCA monitor development - score plot and statistics

"controlled state" [41]. This technique has been widely applied in both univariate as well as multivariate process monitoring applications (see e.g. [41], [42], [43] and the references therein).

In this work, we develop a Shewhart control chart on the 'Model Mismatch' signal (= Calibration model prediction − Soft sensor prediction) for monitoring the HME process in real-time. This chart computes the upper/lower control limits (UCL/LCL) based on the training data as follows [40]:

$$UCL = \mu_m + L\sigma_m \tag{6a}$$

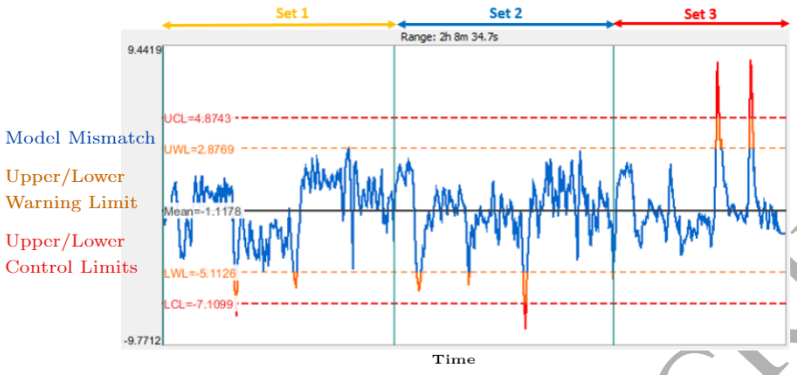

Figure 11: Shewhart Control Chart for SPC Monitoring

$$LCL = \mu_m - L\sigma_m \tag{6b}$$

where μ_m and σ_m represent the mean and standard deviation of process signal m, and $L = 3$ represents the distance away from the mean line. Under the assumption of normally distributed data, with these so-called 'three-sigma' control limits, the Shewhart control chart essentially tests for any changes in the mean (in comparison to the good training data). Shewhart chart, developed using the above DoE training dataset, is shown in Figure 11. It shows the UCL, LCL as well as the warning limits (computed by setting $L = 2$ in equation 6).

4. Real-time Process Monitoring Results

In this section, we present real-time results on the HME system using the developed process monitoring scheme. In particular, results corresponding to commonly occurring HME faults are discussed including feed accumulation issues, Raman probe exposure/calibration faults, barrel zone-heater breakdowns and API impurities/degradation.

4.1. Normal Operating Conditions

When the HME is running under normal operating conditions, there is a good match between the calibration model and soft sensor predictions in both transient and steady-state phases (as shown in Figure 12). This enables the model mismatch signal to remain within its SPC control limits (last plot in

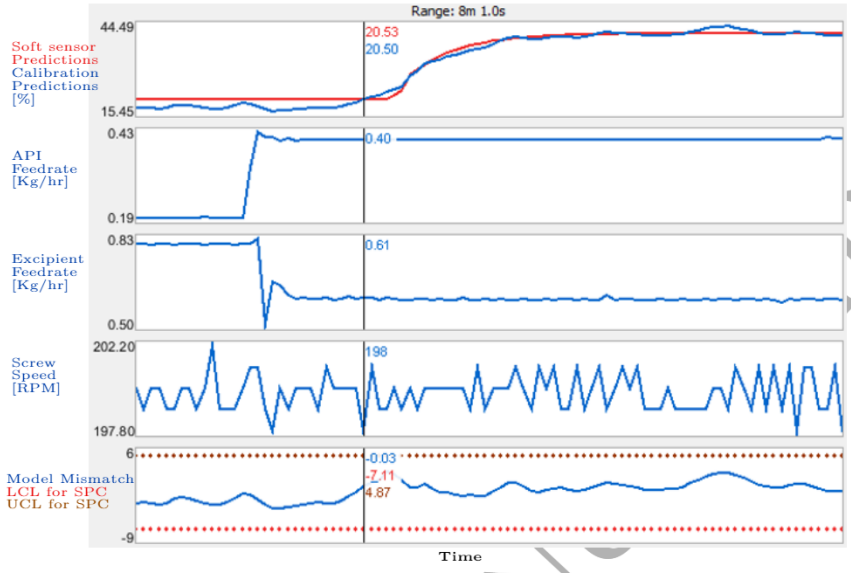

Figure 12: Normal Operation: Process and SPC Data

Figure 12). Furthermore, the SPE and T^2 values being below their respective thresholds for the PCA monitor (last plot in Figure 13) also reflects this state of 'no-fault' operation.

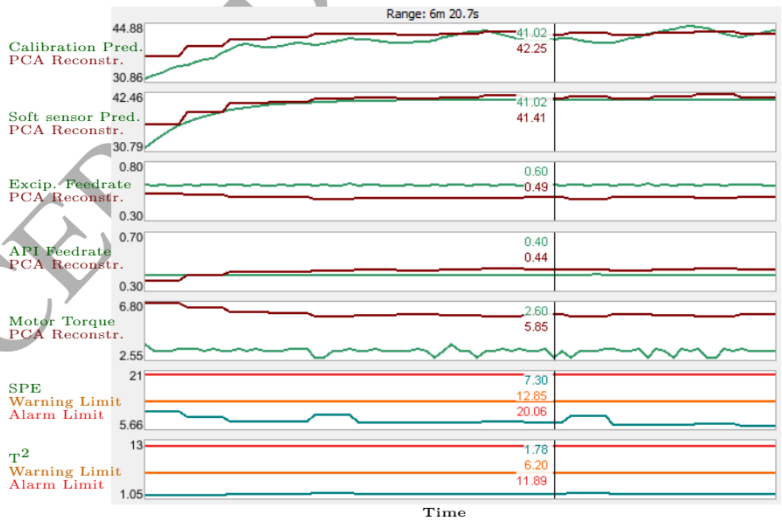

Figure 13: Normal Operation: PCA reconstructions, SPE and T^2 data

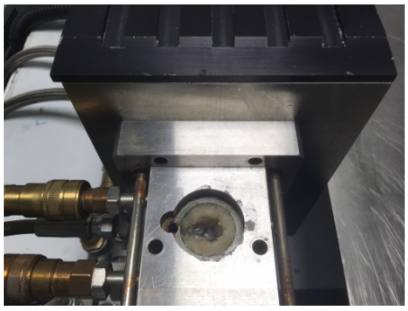

Figure 14: API powder accumulation at the HME feed zone

4.2. API Feeding Issues

We consider the common case of dispensed API powder accumulating in the feed throat of the HME barrel (shown in Figure 14). This is caused by cohesiveness/poor flow-properties of the powder and means that a proportion of the API powder, whilst being dispensed properly, is not moving through the HME barrel towards the die-zone (see also Remark 3). For this case, as shown in Figure 15, the Raman-based calibration model correctly reduces its API concentration predictions, whereas the soft sensor still maintains its prediction of around 41% concentration (as it is based on the feedrate process values coming from the two feeders, which - as shown in plots 2 and 3 of Figure 15 - expectedly remain fairly constant since powder is being correctly delivered out of the feeders). Due to this discrepancy, the mismatch signal falls below the SPC lower control limit (red shaded region in plot 5, Figure 15) with the fault being detected in under 2 minutes (which is comparable to the powder propagation time through the HME barrel, see 5). Due to this breakdown in correlation, the PCA model reconstructions also no longer match the process data resulting in the SPE value exceeding its alarm limit (red shaded region in plot 6, Figure 16).

Once the API accumulation is cleared, the two predictions match-up again resulting in the SPE values going back to normal levels.

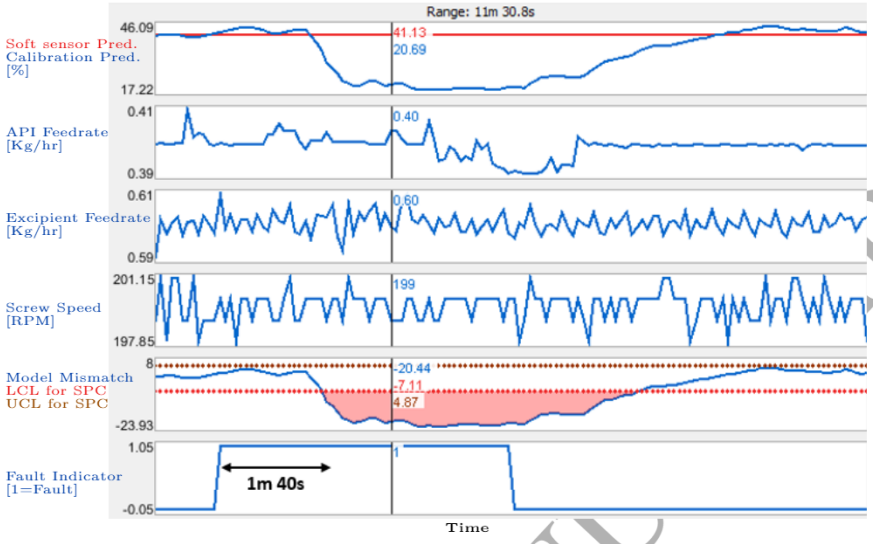

Figure 15: API feeding issues: Process and SPC Data

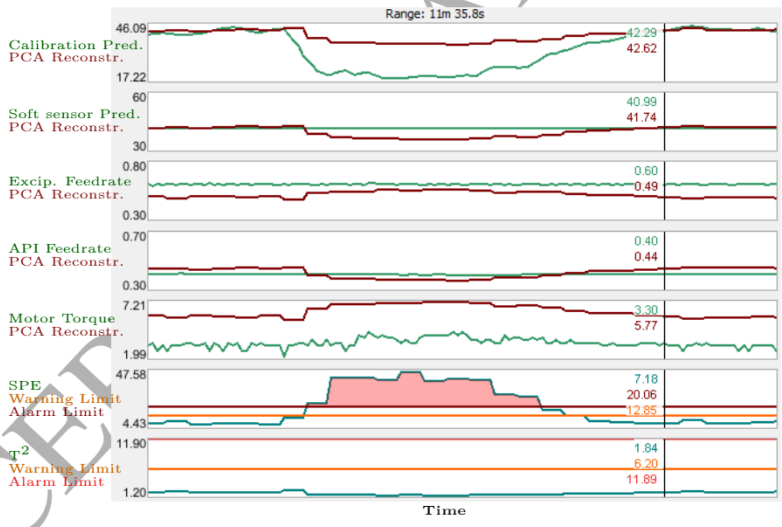

Figure 16: API feeding issues: PCA reconstructions, SPE and T^2 data

Remark 3. *There are a few other common feeding faults which can also be picked up in the same way by the proposed scheme. For instance, during online powder refills and other (vibrational) disturbances to the load cells, the feeders automatically switch from gravimetric (closed-loop) to volumetric (open-loop)*

mode [18]. This frequently causes the feeders to under-deliver powder whilst still (incorrectly) reporting the desired feedrate - thus causing the mismatch. In traditional manufacturing, such faults are picked up much later by the operator whilst the proposed scheme enables automatic, rapid detection within a few minutes. For further details on such faults, see e.g. [44] and the references therein.

4.3. Raman Probe Fault

The Raman probe typically sits flush with the extrudate material in the HME die-zone. This sometimes causes material to deposit on the probe window which in turn affects the spectral signature. Furthermore, Raman spectra is also sensitive to changes in the ambient light conditions and exposure.

Results corresponding to above Raman probe fault are shown in Figure 17. It can be seen that the soft sensor predictions, based on the feedrates, are correct but the calibration model does not properly react to feedrate step-change (plots 2 and 3 in Figure 17). This prediction divergence causes the mismatch signal to drop below the SPC lower control limit (red shaded region) - hence generating the alarm.

Looking at the PCA results in Figure 18, we note that, PCA model (correctly) reconstructs a much higher value for the calibration model predictions based on the real-time HME process data. This discrepancy between the (faulty) Raman calibration model prediction and its PCA reconstruction contributes to the SPE breaching its alarm limit (plot 6, Figure 18).

Remark 4. *Note that whilst one could investigate only the PCA reconstructions of the calibration predictions together with the process data to detect faults, the back-up soft sensor helps to add redundancy to the system and allows for efficient and reliable fault detection, using for instance a simple SPC monitor, based upon the divergence of two independent predictions (see e.g. [7] and the references therein).*

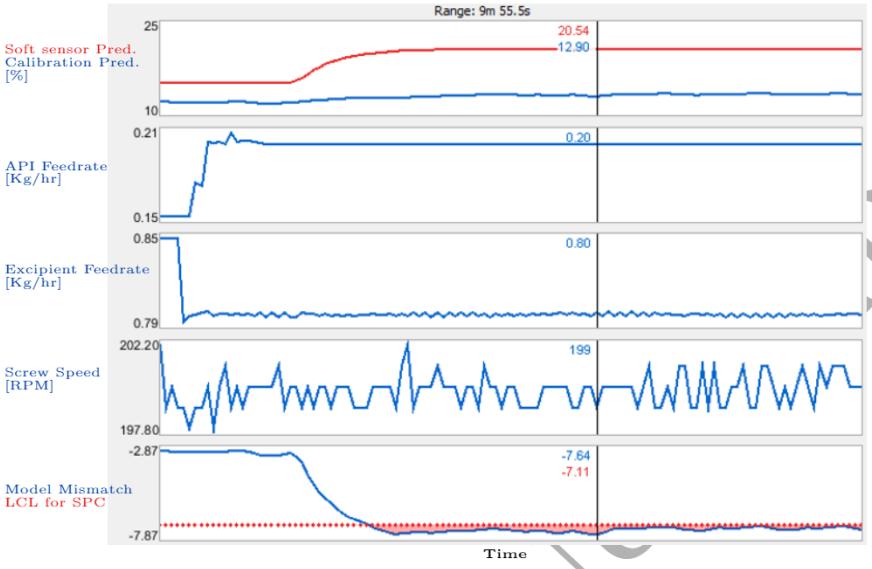

Figure 17: Raman Probe Fault: Process and SPC Data

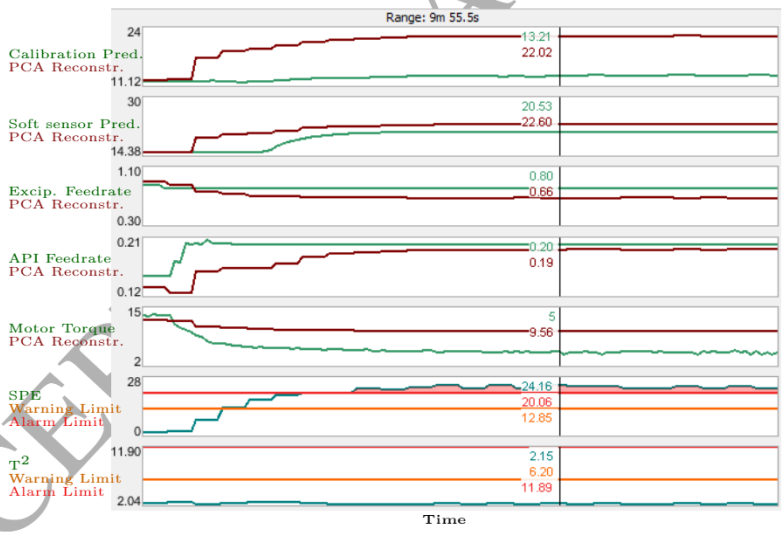

Figure 18: Raman Probe Fault: PCA reconstructions, SPE and T^2 data

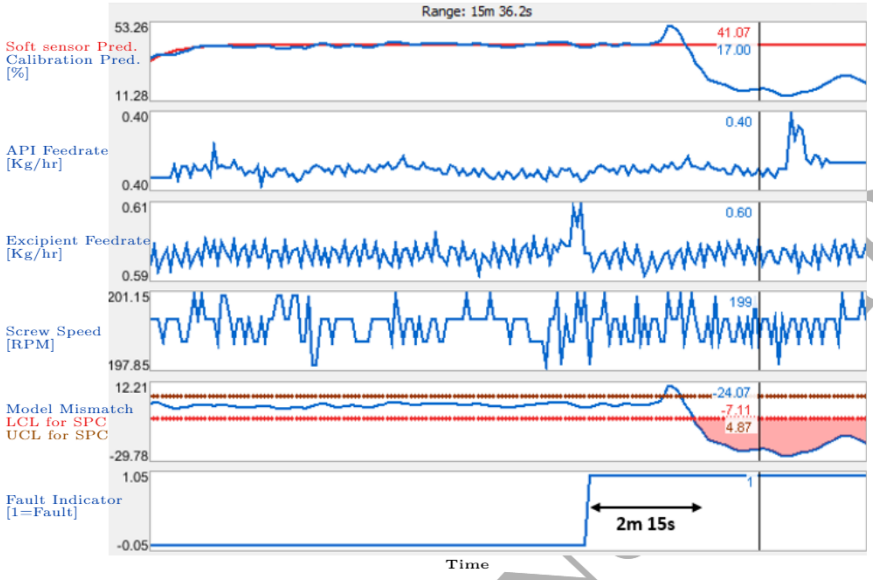

Figure 19: API Impurity: Process and SPC Data

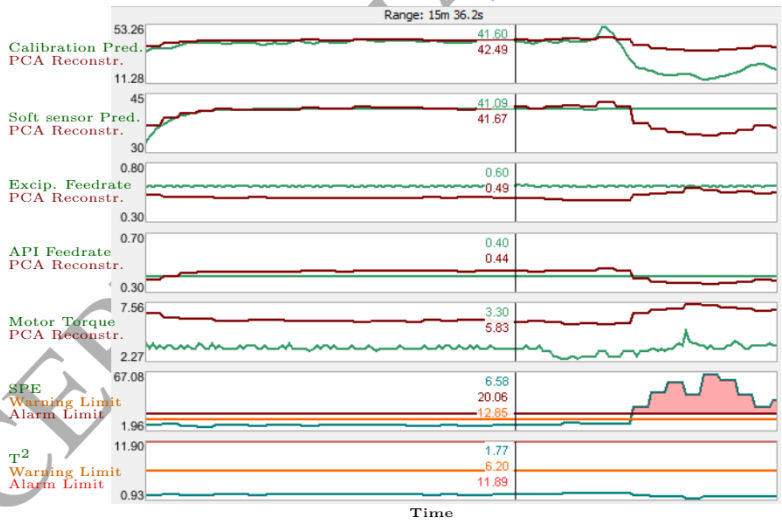

Figure 20: API Impurity: PCA reconstructions, SPE and T^2 data

4.4. API Powder Impurities

Another source of disturbance/uncertainty within HME production is powder impurity/degradation. This is typically caused by grade inconsistencies in

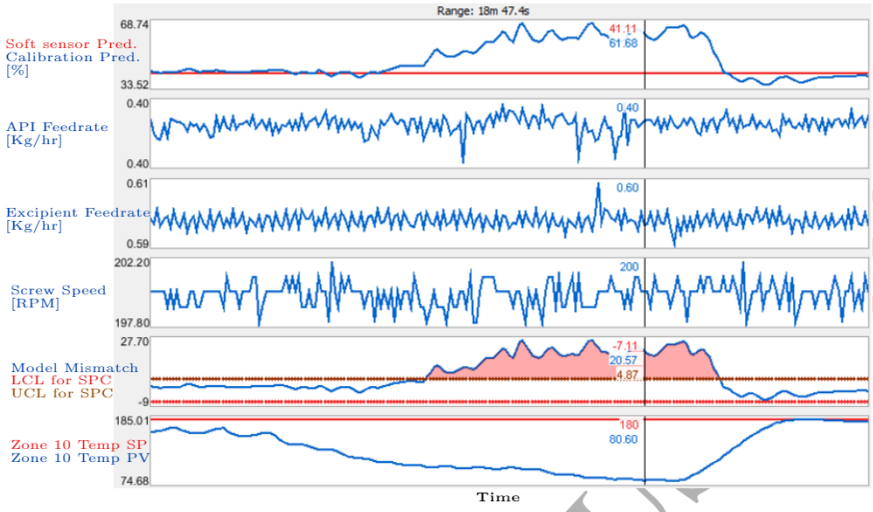

Figure 21: Heater Fault: Process and SPC Data

the powder material received from the supplier, degradation of API due to high extruder shear/heat, and powder contamination during online feeder refills. For this fault, as shown in Figure 19, the calibration model prediction correctly drops (due to to the impurities/degradation). However, the soft sensor predictions, based on the feedrates, do not take account of this. As a result, the mismatch signal goes below the SPC lower control limit after just over two minutes of the fault occurring (plot 5 in Figure 19). Similarly, the PCA model also signals this correlation breakdown as SPE exceeds its alarm limit (as shown in plot 6 of Figure 20).

4.5. Barrel Heater Fault

All the 10 barrel-zones contain separate heating elements to control the material temperature along the HME. As mentioned in section 1, temperature changes affect the API crystallinity/amorphicity structure within the extrudate. These structural changes impacts the corresponding Raman spectral signature and, in turn, the calibration model predictions.

Figure 21 shows the results when zone-10 heater (towards the HME outlet) malfunctions and is unable to maintain its temperature setpoint (SP) value of

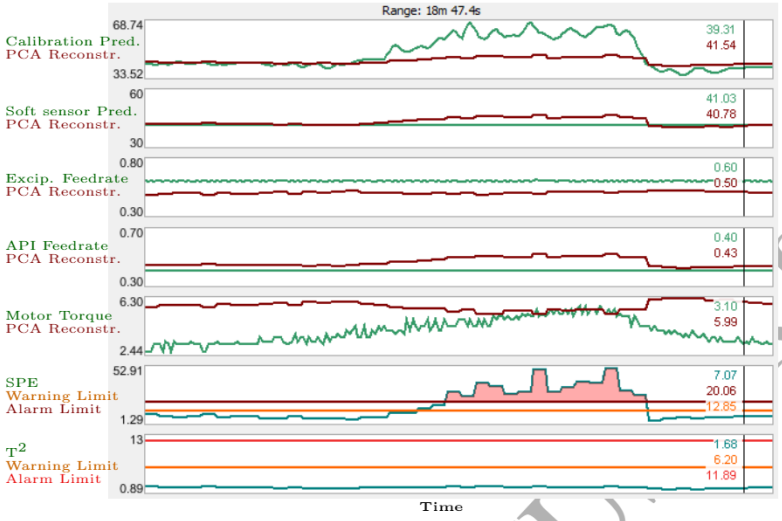

Figure 22: Heater Fault: PCA reconstructions, SPE and T^2 data

180 Deg C (plot 6, Figure 21). The calibration model predictions (erroneously) increase due to the changed spectra associated with a more crystalline extrudate (caused by the zone temperature drop - see [14]). However, the soft sensor predictions remain unchanged (and true) corresponding to constant feedrates. This prediction discrepancy shows up in both the mismatch signal (plot 5, Figure 21) as well as the PCA SPE value (plot 6, Figure 22). As shown in Figures 21 and 22, when the heater fault is fixed, the process goes back in statistical control with key monitoring indicators reverting to normal. Finally, Figure 23 shows the crystalline extrudate that was produced as a result of the heater fault (alongside the normal run product).

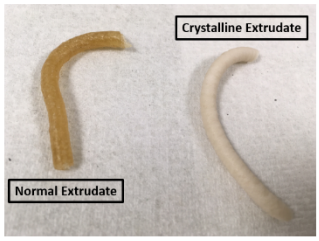

Figure 23: Impact of Heater Fault on the Extrudate

Remark 5. *Whilst the focus of the proposed monitoring scheme is on detection of various common faulty operations, fault isolation capability can be incorporated through the development of nonlinear methods such as Radial Basis Functions (RBF) and Self-Organising Maps (SOM) - see e.g. [10] and the references therein. These Neural Network techniques can be used, together with the PCA monitor, to model the relationship between certain process conditions and the corresponding fault case. Apart from the normal operating data, such models require training on the data for the specific faults to be isolated. Furthermore, additional variables such as die pressure, motor power, and energy/mass balance calculations would also need to be included and this forms part of the future work.*

5. Conclusions

A real-time process monitoring scheme has been proposed for a pharmaceutical HME process. The scheme involves PCA and SPC monitors using process data as well as the concentration predictions from two independent soft sensors to detect different types of common faults during manufacturing, in real-time.

The novelty of this work lies in the design and application of a two-sensor framework to process monitoring. The calibration model (based on the Raman spectra) and hybrid soft sensor (based on feeder process data) both independently predict the API concentration at the HME outlet. As demonstrated through the real-time extrusion results, the prediction mismatch from these two sensors enables the PCA/SPC monitors to automatically detect various types of process faults (e.g. zone-heater breakdowns, feeding issues and powder impurities/degradation) which would otherwise remain undetected with a single-sensor monitoring scheme. Furthermore, the mismatch signal and correlation breakdown also provide other fault information, including the occurrence time.

Acknowledgements

We would like to thank the Reviewers for their comments which have helped to improve the paper.

Funding for this work from Advanced Manufacturing Supply Chain Initiative (AMSCI), as part of the REMEDIES project, is gratefully acknowledged. We are also grateful to Dow Chemical Company for the complimentary supply of Affinisol powder. Finally, CMAC National Facility is supported by UKRPIF (UK Research Partnership Fund) award from the Higher Education Funding Council for England (HEFCE) (Grant ref HH13054).

References

[1] M. Maniruzzaman, J. S. Boateng, M. J. Snowden, D. Douroumis, A review of hot-melt extrusion: process technology to pharmaceutical products, ISRN pharmaceutics 2012.

[2] D. Markl, P. R. Wahl, J. C. Menezes, D. M. Koller, B. Kavsek, K. Francois, E. Roblegg, J. G. Khinast, Supervisory control system for monitoring a pharmaceutical hot melt extrusion process, AAPS PharmSciTech 14 (3) (2013) 1034–1044.

[3] L. Saerens, C. Vervaet, J. P. Remon, T. De Beer, Process monitoring and visualization solutions for hot-melt extrusion: a review, Journal of Pharmacy and Pharmacology 66 (2) (2014) 180–203.

[4] M. Maniruzzaman, D. Douroumis, Continuous manufacturing and process analytical tools, International journal of pharmaceutics 496 (1) (2015) 1–2.

[5] M. A. Repka, S. Majumdar, S. Kumar Battu, R. Srirangam, S. B. Upadhye, Applications of hot-melt extrusion for drug delivery, Expert opinion on drug delivery 5 (12) (2008) 1357–1376.

[6] M. Wilson, M. A. Williams, D. S. Jones, G. P. Andrews, Hot-melt extrusion technology and pharmaceutical application, Therapeutic delivery 3 (6) (2012) 787–797.

[7] P. Kadlec, B. Gabrys, S. Strandt, Data-driven soft sensors in the process industry, Computers & chemical engineering 33 (4) (2009) 795–814.

[8] Z. X. Wang, Q. P. He, J. Wang, Comparison of variable selection methods for pls-based soft sensor modeling, Journal of Process Control 26 (2015) 56–72.

[9] Z. Ge, Review on data-driven modeling and monitoring for plant-wide industrial processes, Chemometrics and Intelligent Laboratory Systems 171 (2017) 16–25.

[10] P. Kämpjärvi, M. Sourander, T. Komulainen, N. Vatanski, M. Nikus, S.-L. Jämsä-Jounela, Fault detection and isolation of an on-line analyzer for an ethylene cracking process, Control engineering practice 16 (1) (2008) 1–13.

[11] J. Van Renterghem, A. Kumar, C. Vervaet, J. P. Remon, I. Nopens, Y. Vander Heyden, T. De Beer, Elucidation and visualization of solid-state transformation and mixing in a pharmaceutical mini hot melt extrusion process using in-line raman spectroscopy, International journal of pharmaceutics 517 (1) (2017) 119–127.

[12] V. S. Tumuluri, M. S. Kemper, I. R. Lewis, S. Prodduturi, S. Majumdar, B. A. Avery, M. A. Repka, Off-line and on-line measurements of drug-loaded hot-melt extruded films using raman spectroscopy, International journal of pharmaceutics 357 (1) (2008) 77–84.

[13] L. Saerens, L. Dierickx, B. Lenain, C. Vervaet, J. P. Remon, T. De Beer, Raman spectroscopy for the in-line polymer–drug quantification and solid state characterization during a pharmaceutical hot-melt extrusion process, European Journal of Pharmaceutics and Biopharmaceutics 77 (1) (2011) 158–163.

[14] A. Almeida, L. Saerens, T. De Beer, J. P. Remon, C. Vervaet, Upscaling and in-line process monitoring via spectroscopic techniques of ethylene vinyl acetate hot-melt extruded formulations, International journal of pharmaceutics 439 (1) (2012) 223–229.

[15] L. Saerens, C. Vervaet, J.-P. Remon, T. De Beer, Visualization and process understanding of material behavior in the extrusion barrel during a hot-melt extrusion process using raman spectroscopy, Analytical chemistry 85 (11) (2013) 5420–5429.

[16] L. Fortuna, S. Graziani, A. Rizzo, M. G. Xibilia, Soft sensors for monitoring and control of industrial processes, Springer Science & Business Media, 2007.

[17] Thermo Fisher Scientific, Karlsruhe, Germany, http://www.thermofisher.com.

[18] M. Hopkins, Loss in weight feeder systems, Measurement and Control 39 (8) (2006) 237–240.

[19] Brabender Technologies, Ontario, Canada, http://www.brabender-technologie.com/en/.

[20] Kaiser Optical Systems, Michigan, USA, http://www.kosi.com/na_en/.

[21] Perceptive Engineering Limited, Daresbury, UK, http://www.perceptiveapc.com.

[22] OPC Foundation, https://opcfoundation.org/about/what-is-opc/.

[23] S. Yin, S. X. Ding, A. Haghani, H. Hao, P. Zhang, A comparison study of basic data-driven fault diagnosis and process monitoring methods on the benchmark tennessee eastman process, Journal of Process Control 22 (9) (2012) 1567–1581.

[24] S. Joe Qin, Statistical process monitoring: basics and beyond, Journal of chemometrics 17 (8-9) (2003) 480–502.

[25] V. Venkatasubramanian, R. Rengaswamy, S. N. Kavuri, K. Yin, A review of process fault detection and diagnosis: Part iii: Process history based methods, Computers & chemical engineering 27 (3) (2003) 327–346.

[26] S. Ding, P. Zhang, E. Ding, S. Yin, A. Naik, P. Deng, W. Gui, On the application of pca technique to fault diagnosis, Tsinghua Science & Technology 15 (2) (2010) 138–144.

[27] G. Chen, T. J. McAvoy, M. J. Piovoso, A multivariate statistical controller for on-line quality improvement, Journal of Process Control 8 (2) (1998) 139–149.

[28] J. Flores-Cerrillo, J. F. MacGregor, Control of batch product quality by trajectory manipulation using latent variable models, Journal of Process Control 14 (5) (2004) 539–553.

[29] J. E. Jackson, G. S. Mudholkar, Control procedures for residuals associated with principal component analysis, Technometrics 21 (3) (1979) 341–349.

[30] N. D. Tracy, Multivariate control charts for individual observations, Jour. Quality Technology 24 (2) (1992) 88–95.

[31] P. Geladi, B. R. Kowalski, Partial least-squares regression: a tutorial, Analytica chimica acta 185 (1986) 1–17.

[32] K. S. Ng, A simple explanation of partial least squares (2013).

[33] S. Wold, M. Sjöström, L. Eriksson, Pls-regression: a basic tool of chemometrics, Chemometrics and intelligent laboratory systems 58 (2) (2001) 109–130.

[34] Å. Rinnan, F. van den Berg, S. B. Engelsen, Review of the most common pre-processing techniques for near-infrared spectra, TrAC Trends in Analytical Chemistry 28 (10) (2009) 1201–1222.

[35] C. Shende, W. Smith, C. Brouillette, S. Farquharson, Drug stability analysis by raman spectroscopy, Pharmaceutics 6 (4) (2014) 651–662.

[36] B. Hernández, F. Pflüger, S. G. Kruglik, M. Ghomi, Characteristic raman lines of phenylalanine analyzed by a multiconformational approach, Journal of Raman Spectroscopy 44 (6) (2013) 827–833.

[37] F. R. Dollish, W. G. Fateley, F. F. Bentley, Characteristic Raman frequencies of organic compounds, Wiley, 1974.

[38] R. M. Felder, R. W. Rousseau, L. G. Bullard, Elementary Principles of Chemical Processes, Wiley, 2016.

[39] L. Ljung, System identification: Theory for the user, ptr prentice hall information and system sciences series, ed: Prentice Hall, New Jersey, 1999.

[40] D. C. Montgomery, Introduction to statistical quality control, John Wiley & Sons, 2007.

[41] J. F. MacGregor, T. Kourti, Statistical process control of multivariate processes, Control Engineering Practice 3 (3) (1995) 403–414.

[42] T. Kourti, Application of latent variable methods to process control and multivariate statistical process control in industry, International Journal of adaptive control and signal processing 19 (4) (2005) 213–246.

[43] M. Xie, T. N. Goh, P. Ranjan, Some effective control chart procedures for reliability monitoring, Reliability Engineering & System Safety 77 (2) (2002) 143–150.

[44] W. E. Engisch, F. J. Muzzio, Feedrate deviations caused by hopper refill of loss-in-weight feeders, Powder Technology 283 (2015) 389–400.

[45] N. Langley, J. DiNunzio, M. A. Repka, Melt Extrusion: Materials, Technology and Drug Product Design (AAPS Advances in the Pharmaceutical Sciences Series), Springer, 2013.

Appendix: Hybrid Soft Sensor Model

In this Appendix, we present a proof sketch for the FOPTD model given in equation (4), based on the principles of (component) mass balance [38].

During normal steady state operation, the mass flow at the inlet and outlet of the HME barrel is the same which implies negligible powder build-up within the unit [45]. Then, denoting the API feedrate by F_{API}, and total inlet and outlet feedrates by F_{in} and F_{out}, respectively, all in kg/hr, we can write:

$$F_{in}(t) = F_{out}(t) \implies \frac{dM_b(t)}{dt} = 0 \tag{7}$$

where $M_b(t)$, in kg, denotes the powder mass in the HME barrel at time t.

Let C_{in} and C_{out} respectively denote the inlet and outlet concentration ratios (unitless) defined by:

$$C_{in}(t) := \frac{F_{API}(t)}{F_{in}(t)}, \qquad C_{out}(t) := \frac{F_{API}(t)}{F_{out}(t)} \tag{8}$$

Then, applying the principles of component mass balance for the API, it follows that

$$F_{API}(t) - F_{out}(t).C_{out}(t) = M_b \frac{dC_{out}(t)}{dt} \tag{9}$$

In (9), replacing $F_{out}(t)$ by $F_{in}(t)$ (as specified in equation (7)) and dividing both sides by $F_{in}(t)$ yields the (CSTR) differential equation:

$$C_{in}(t) - C_{out}(t) = T \frac{dC_{out}(t)}{dt} \tag{10}$$

where T, the time constant reflective of the mean residence time, is given by:

$$T := \frac{M_b}{F_{in}} \tag{11}$$

Note that the model in (10) assumes perfect mixing (a standard assumption for CSTR). Therefore, to take account of the material propagation delay through the HME barrel, we add a plug flow component to the C_{in} term in the model. Furthermore, a gain term (K) is incorporated to not only obtain the output concentration C_{out} as percentage value (denoted by $C^p_{out}(s)$), but also to provide an extra degree of freedom for fitting the model to calibration prediction data

as part of model development process. Finally, taking the Laplace transform of this modified system yields the transfer function:

$$G(s) = \frac{C^p_{out}(s)}{C_{in}(s)} = \frac{Ke^{-ds}}{Ts+1}$$